

1 **Risk-based hydrologic design under climate change using stochastic weather**  
2 **and watershed modeling**

3

Ghazal Shabestanipour<sup>1</sup>, Zachary Brodeur<sup>2</sup>, Benjamin Manoli<sup>1</sup>, Abigail Birnbaum<sup>1</sup>, Scott  
Steinschneider<sup>2</sup>, and Jonathan R. Lamontagne<sup>1\*</sup>

September 13, 2023

1. Department of Civil & Environmental Engineering, Tufts University, Medford, MA, USA
  2. Department of Biological & Environmental Engineering, Cornell University, Ithaca, NY, USA
- \* Corresponding author.

4

5

**Abstract**

6

7 Water resources planning and management requires the estimation of extreme design events.  
8 Anticipated climate change is playing an increasingly prominent role in the planning and design  
9 of long-lived infrastructure, as changes to climate forcings are expected to alter the distribution  
10 of extremes in ways and to extents that are difficult to predict. One approach is to use climate  
11 projections to force hydrologic models, but this raises two challenges. First, global climate  
12 models generally focus on much larger scales than are relevant to hydrologic design, and  
13 regional climate models that better capture small scale dynamics are too computationally  
14 expensive for large ensemble analyses. Second, hydrologic models systematically misrepresent  
15 the variance and higher moments of streamflow response to climate, resulting in a  
16 mischaracterization of the extreme flows of most interest. To address both issues, we propose a  
17 new framework for non-stationary risk-based hydrologic design that combines a stochastic  
18 weather generator (SWG) that accurately replicates basin-scale weather and a stochastic  
19 watershed model (SWM) that accurately represents the distribution of extreme flows. The joint  
20 SWG-SWM framework can generate large ensembles of future hydrologic simulations under  
21 varying climate conditions, from which design statistics and their uncertainties can be estimated.  
22 The SWG-SWM framework is demonstrated for the Squannacook River in the Northeast United

23 States. Standard approaches to design flows, like the  $T$ -year flood, are difficult to interpret under  
24 non-stationarity, but the SWG-SWM simulations can readily be adapted to risk and reliability  
25 metrics which bare the same interpretation under stationary and non-stationary conditions. As an  
26 example, we provide an analysis comparing the use of risk and more traditional  $T$ -year design  
27 events, and conclude that risk-based metrics have the potential to reduce regret of over- and  
28 under-design compared to traditional return-period based analyses.

29

## 30 **1. Introduction**

31 Water resources infrastructure is generally designed to manage hydrologic extremes.  
32 Conventionally, such designs have leveraged historical extreme events to estimate the magnitude  
33 of future extremes associated with some annual exceedance probability (AEP). For instance,  
34 design floods and design storms associated with different return periods are commonly used to  
35 size infrastructure (Haghighatafshar et al. 2020), and such analyses form the basis of standard  
36 design criteria in many countries (e.g., Bulletin 17C). Here, a flood or storm magnitude  
37 associated with the  $T$ -year return period (or recurrence interval) is an event with a  $p = 1/T$  AEP  
38 (Gumbel 1941). The terms ‘return period’ and ‘recurrence interval’ arise because  $T$  is the  
39 average time until a  $T$ -year event is exceeded, assuming the events are independent and  
40 stationary (Stedinger 1993).

41 However, climate change complicates water resources planning in general, and the use of  
42 design events and return periods in particular. Human-induced climate change is expected to  
43 have various impacts on atmospheric and hydrologic systems, such as intensified and  
44 intermittent precipitation (Intergovernmental Panel On Climate Change (IPCC) 2023), changes  
45 in snow accumulation and timing, unprecedented rates of snow and glacier melt (Pörtner et al.  
46 2022), sea level rise (Oki and Kanae 2006), and longer droughts and dry periods due to increased  
47 potential evapotranspiration and decline in soil moisture (Balting et al. 2021), among others.

48 These climate impacts are expected to alter the distribution of hydrologic extremes over time as  
49 the Earth continues to warm. Mapping changes in climate drivers to changes in hydrologic  
50 extremes is challenging because of the complicated and nonlinear nature of the hydrologic cycle  
51 and the path dependence of extreme events (Vogel 2017).

52 Even if it is possible to estimate the evolution of non-stationary hydrologic extremes,  
53 Read and Vogel (2015) raised several concerns with the use of return periods and AEPs in  
54 hydrologic design in a non-stationary world. First, the interpretation of a return period is  
55 ambiguous when the AEP associated with a design flow is changing over time, and alternative  
56 definitions have been proposed. Read and Vogel (2015) show that the mean and distribution of  
57 the actual return period of a design event changes substantially as a function of the long-term  
58 trend in the annual maximum series, its variability, and the severity of the design event. If the  
59 annual maximum series is increasing over time, the relative reduction in the true return period of  
60 a design flow increases with the extremity of the design flow. For example, the true return period  
61 of the stationary 100-year flood will decrease relatively more than the true return period of the  
62 stationary 10-year flood.

63 Read and Vogel 2015, Fernández and Salas 1999, and Pielke 1999 have also critiqued the  
64 use of return periods and AEPs in design under stationary conditions. In addition to a general  
65 misunderstanding of their meaning by practitioners and the public alike (Fernández and Salas  
66 1999; Pielke 1999; Douglas, Vogel, and Kroll 2002; Cooley 2012; Serinaldi 2015; Serinaldi and  
67 Kilsby 2015), return periods and AEPs do not account for the design-life of the structure  
68 (Haghighatafshar et al. 2020), and so do not directly relate the risk-of-failure or reliability of a  
69 design over its intended design life. The lifetime risk of failure is likely of more use to planners

70 and engineers than the average return period or one year AEP. This problem only compounds  
71 when the likelihood of extremes changes over time under climate change.

72 An alternative approach for water resources infrastructure design that is more suitable  
73 under non-stationarity is design-life specific risk or reliability. Here risk is defined as the  
74 probability a critical threshold is exceeded over the design-life, and reliability is the probability  
75 the critical threshold is not exceeded (reliability = 1-risk). Thus, the calculation is tailored  
76 towards the question: how likely is it that a project will fail over a T-year planning horizon?  
77 Engineers can then size, design, and manage infrastructure to meet a pre-selected level of risk  
78 deemed acceptable. Even if the probability of extremes evolves over the planning horizon, as is  
79 expected under climate change, the risk of project failure can still be presented as a single design  
80 value, assuming the time-varying distribution of extremes is integrated into the calculation of  
81 risk. This is in contrast to the traditional planning approaches that use design events for specific  
82 return periods. Return periods do not account for climate change dynamic impacts on hydrologic  
83 processes that govern extreme events. Under these approaches, engineers would first need to  
84 select both a return period and a future target year before calculating the associated design event  
85 and would still face the challenge of resolving the meaning of that return period as the likelihood  
86 of extremes changes over the planning horizon (e.g., Salas and Obeysekera 2014).

87 Despite the potential benefits of design-life specific risk as a criterion to guide  
88 infrastructure planning under climate change, there are several challenges in calculating this risk.  
89 Ideally, an analyst would have access to a very large ensemble of transient climate traces that 1)  
90 were unbiased with respect to key meteorological characteristics that impact hydrologic extremes  
91 (e.g., the space-time distribution of precipitation across multiple temporal and spatial scales); and  
92 2) encompassed the full range of plausible future climate conditions with an accurate

93 representation of the likelihood of different climate states in the future. If such ensembles were  
94 available, they could be used to estimate the risk of failure over a planning period of interest.  
95 Unfortunately, neither of these conditions usually holds.

96         First, the current generation of global climate models (GCMs) remain biased with respect  
97 to key aspects of local weather, and statistically correcting these biases remains challenging.  
98 Changes to atmospheric dynamics can play a critical role in regional climate change (Lu et al.  
99 2014; O’Gorman 2015), but there is significant bias in the representation of major patterns of  
100 atmospheric circulation in GCMs, complicating the direct use of precipitation projections  
101 (Hawcroft et al. 2018; Woollings 2010; Zappa, Shaffrey, and Hodges 2013; Stephenson et al.  
102 2012; Kyselý et al. 2016; Tan et al. 2018). Statistical correction of dynamical biases is difficult  
103 since they are linked to modeled physical processes that could change under warming, thus  
104 changing the bias over time (Stephenson et al. 2012; Muñoz et al. 2017; Maher et al. 2019). In  
105 addition, the coarse spatial resolution of GCMs can introduce additional biases into precipitation  
106 extremes. While higher resolution climate models can help address these biases (Kendon et al.  
107 2017), the increase in computational expense precludes large enough ensembles for risk-based  
108 planning (Tebaldi, Snyder, and Dorheim 2022; Steinschneider et al. 2019). Furthermore, even  
109 large GCM ensembles often cannot provide a formal estimate of probability of future climate  
110 states, as they represent the lower bound of future climate uncertainty (Stainforth et al. 2007) and  
111 depend on emissions scenarios that are inherently non-probabilistic. In response, some have  
112 argued for the use of stochastic weather generators (SWGs) to efficiently generate very large  
113 ensembles of future climate (100s of ensemble members, each decades-centuries long) for use in  
114 hydrologic design exercises (Fowler, Blenkinsop, and Tebaldi 2007; Steinschneider et al. 2019;  
115 Daniel S Wilks and Wilby 1999; Richardson 1981). These models, which are trained to historical

116 weather data, can produce scenarios that are by design unbiased in key attributes of weather such  
117 as extreme events, but that also can span a very wide but plausible range of future climate change  
118 to ensure that key vulnerabilities are identified.

119           Beyond the challenge of future climate data to support design-life specific risk  
120 estimation, there is also the need to use rainfall-runoff or other hydrologic models to convert  
121 future climate into hydrologic variables of interest for design. Hydrologic models are needed to  
122 capture the complicated relationship between changes in climatic conditions and hydrologic  
123 response, which is a function of complicated, non-linear dynamics and depends on other factors  
124 like antecedent conditions (Sharma, Wasko, and Lettenmaier 2018). In other words, it is not as  
125 simple as noting that an increase of X% in rainfall intensity will result in an increase of Y% in  
126 flood magnitude. However, deterministic hydrologic models usually underrepresent the variance  
127 and asymmetry of daily streamflow, which results in a systematic mischaracterization of the  
128 hydrologic extremes of most interest to engineers and planners (Farmer and Vogel 2016). As a  
129 result, hydrologic simulations of future conditions are likely to mischaracterize hydrologic  
130 extremes under climate change. Farmer and Vogel (2016) attribute this systematic error to a  
131 general failure to account for the variability contained in the model residuals when simulating  
132 from hydrologic models. Vogel (2017) coined the term stochastic watershed models (SWM) for  
133 the approach that adds stochastic error to hydrologic simulations. SWMs have been shown to  
134 improve the representation of hydrologic extremes as compared to their deterministic  
135 counterparts (Shabestanipour et al. 2023), and thus present a promising approach for projecting  
136 future hydrologic extremes under climate change. A hydrologic model's predictive uncertainty is  
137 due to model structure, parameter uncertainties, calibration, and input data (Moges et al. 2020).  
138 Shabestanipour et al. (2023) suggest that assuming that the impact of all sources of uncertainty

139 are contained in the residuals is an effective approach to propagate uncertainty in  
140 characterization of extreme flows (see also Koutsoyiannis and Montanari 2022). While SWMs  
141 are effective at addressing structural uncertainties in a hydrologic model, they need to be  
142 integrated with multiple input scenarios in order to capture changes caused by warmer climates  
143 or land use change.

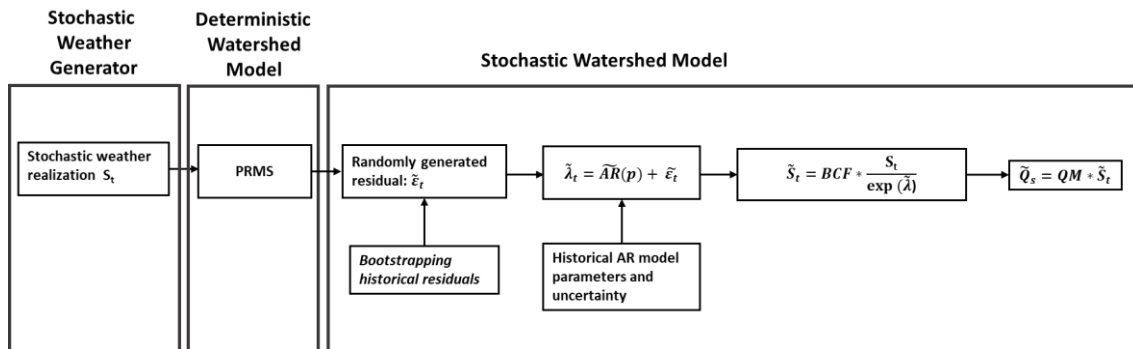
144 In response to the challenges above, this study contributes a framework for risk-based  
145 decision making for water resources infrastructure planning under climate change. This  
146 framework pairs a stochastic weather generator (SWG) with a stochastic watershed model  
147 (SWM) to provide large ensembles of streamflow simulations reflecting varying levels of  
148 potential future warming. Using these ensembles, it is possible to compute risk- and reliability-  
149 based design criterion that reflect the infrastructure’s design life and the appropriate risk-of-  
150 failure under alternative future climate scenarios. The framework also allows planners to project  
151 the evolution of key design criteria, such as critical flood or low flow statistics, over the 21<sup>st</sup>  
152 century under alternative climate scenarios. We apply the proposed framework to the  
153 Squannacook River in Massachusetts to illustrate the changes in critical design statistics under  
154 varying levels of climate change and the application of risk-based metrics to engineering design.

155

## 156 **2. Methodology**

157 The approach detailed in this work is composed of four primary components (see *Figure*  
158 *1*). First, a SWG is used to develop ensembles of future climate scenarios associated with  
159 different signals of climate change. These ensembles are used to force a deterministic watershed  
160 model (DWM), creating ensembles of future streamflow. Ensembles of hydrologic model error  
161 are then sampled and added to each streamflow trace from the DWM, to create an ensemble of

162 ensembles (or super ensemble) of future streamflow traces that capture various signals of climate  
 163 change as well as the effects of hydrologic model uncertainty. Finally, this super ensemble is  
 164 used to calculate the risk-of-failure for water resources infrastructure associated with a  $T$ -year  
 165 design life. After introducing the case study basin used in this work, we describe each of these  
 166 framework components in more detail in the sections below.



167  
 168 **Figure 1:** Integrated Stochastic Weather Generator (SWG)-Stochastic Watershed Model (SWM)  
 169 framework to estimate hydrologic risk under climate change.

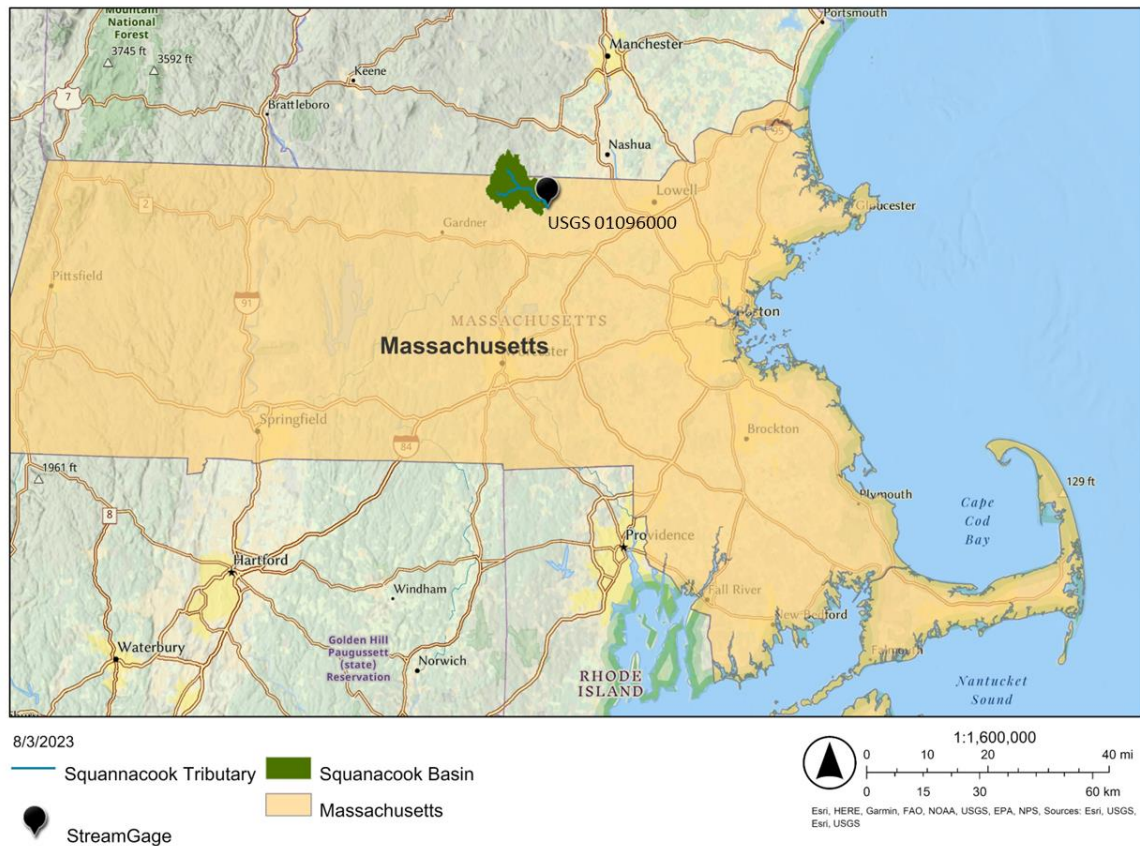
170  
 171 **2.1. Study Basin**

172 We demonstrate the proposed framework for the Squannacook River basin located in  
 173 north-central Massachusetts and southern New Hampshire in the United States (see *Figure 2*). To  
 174 demonstrate SWG-SWM framework’s generalizability, the SWG-SWM procedure was applied  
 175 to a second basin (Shasta River basin, California, United States), with an alternative DWM, and  
 176 different climate realizations. The results of that analysis are reported in the supplementary  
 177 material. Previous studies suggest that the Northeast United States will experience the largest  
 178 temperature increases in the contiguous United States (Hayhoe et al. 2018). Furthermore, a  
 179 recent study in the state of Massachusetts projected an increase of more than 50% in the 100-year  
 180 24-hour rainfall event for much of the state under both RCP4.5 and RCP8.5 emission scenarios

181 (Siddique and Palmer 2021). The Squannacook River basin was selected because it contains a  
182 72-year continuous daily streamflow record, has relatively low regulation and hydrologic  
183 disturbance, and served as a pilot study for a previous SWM demonstration project  
184 (Shabestanipour et al. 2023).

185         The Squannacook River drains southeasterly into the Nashua River, which in turn flows  
186 to the Merrimack River watershed and ultimately the Atlantic Ocean. The portion of the  
187 Squannacook River basin modeled in this study corresponds to the USGS streamgage 01096000,  
188 which has a drainage area of 173.8 km<sup>2</sup>. The watershed is primarily forested and contains more  
189 than 28 km<sup>2</sup> of state and town forests. There are developed areas along key transportation  
190 corridors and in the center of Townsend, Massachusetts. Less than 8% of this basin area is  
191 impervious and it contains five dams. The basin topography ranges from a hilly upland plateau  
192 with maximum elevation of 450 m in the north and west to flat coastal plain in the south and  
193 east.

## Squannacook



194

195 **Figure 2:** Location of the Squannacook River basin in Massachusetts, USA.

196

197 The climate in the Squannacook River basin is temperate, with mild summers and cold  
198 winters. The mean annual air temperature during 1981–2010 was about 46 °F (7.78 °C) with mean  
199 monthly air temperatures ranging from about 22 °F (-5.5 °C) in January to 69 °F (20.5 °C) in July  
200 (ETOPO 2022 15 Arc-Second Global Relief Model). The mean annual precipitation is 48 inches  
201 (1219 mm) (ETOPO 2022 15 Arc-Second Global Relief Model), while the basin’s average annual  
202 potential evapotranspiration for the period of 1981–2010 is 23 inches (584 mm) (Northeast  
203 Regional Climate Center, 2021).

204 The DWM used in this pilot study is the USGS National Hydrologic Model Precipitation  
205 Runoff Modeling System (NHM-PRMS) version 5.1.0 (Markstrom et al. 2015; Regan et al. 2019).  
206 NHM-PRMS is a medium-complexity continuous watershed simulation model that is calibrated  
207 for the entire continental United States (Regan et al. 2019). The DAYMET climate dataset  
208 (Thornton et al. 2016) and available USGS streamflow records were used to configure and  
209 calibrate the NHM-PRMS. Calibration of NHM-PRMS is accomplished through a normalized  
210 squared error on streamflow along several calibration steps (e.g., high flows, low flows, monthly  
211 flows, and daily flows) for hydrologic response units. See Regan et al. (2019) for a full description  
212 of the calibration procedure. Minimal modification to the NHM-PRMS calibration was performed  
213 for this pilot study, including adjustment factors for minimum and maximum temperature,  
214 precipitation, precipitation-to-snow conversion, monthly air temperature coefficients used for  
215 potential evapotranspiration, and the groundwater discharge coefficient. The performance of the  
216 model in the Squannacook is adequate, with a Nash Sutcliffe efficiency of 0.64 and a log Nash  
217 Sutcliffe efficiency of 0.71. This is very similar to the average performance of PRMS across the  
218 United States (Farmer and Vogel 2016).

219

## 220 **2.2. Stochastic Weather Generator and Climate Scenarios**

221 Stochastic weather generators provide a computationally efficient and complementary  
222 alternative to GCMs for hydrologic systems' analysis under climate change. These models are  
223 structured based on historical meteorological records and are used to generate large ensembles of  
224 simulated daily weather records that are similar to but not bound by variability in past  
225 observations (Richardson, 1981; Wilks and Wilby, 1999; Fowler et al. 2007). For hydrologic  
226 impact assessment studies, weather generators must develop timeseries of multiple weather

227 variables (e.g., precipitation and temperature) at multiple locations while maintaining the  
228 persistence and covariance structures associated with transient, multi-day storm events and over  
229 longer (seasonal-inter-annual) timescales. After a weather generator has been calibrated to  
230 historical data, model parameters can be adjusted to produce new realizations of weather,  
231 presenting changes in intensity and frequency of average and extreme precipitation, heatwaves,  
232 and cold spells (Wilks 2002; Wilks 2010; Wilks 2012) The reasoning behind the specific  
233 methodological choices in the SWG used in this study are described in (Najibi and  
234 Steinschneider 2023).

235         We adopt the SWG developed for the state of Massachusetts by Steinschneider and  
236 Najibi (2022). This SWG is based on the model described in Steinschneider et al. (2019), Rahat  
237 et al. (2022), and Najibi, Mukhopadhyay, and Steinschneider (2021). An advantage of the SWG  
238 over direct use of GCM projections, is the ability of the SWG to produce a larger number of  
239 climate change realizations at a spatial and temporal scale that is meaningful for hydrologic  
240 simulation, than what is typically available through direct use of downscaled GCMs. This  
241 weather generator is a semiparametric, multivariate, and multisite model that is designed to  
242 separately model dynamic and thermodynamic atmospheric mechanisms of climate variability  
243 and change through statistical abstractions of these processes. To capture atmospheric dynamics,  
244 the weather generator uses a non-homogenous Hidden Markov Model (NHMM) to identify and  
245 simulate sequences of weather regimes (WRs), which are recurring large-scale atmospheric flow  
246 patterns (e.g., upper-level, quasi-stationary blocks and troughs) that organize high-frequency  
247 weather systems (Robertson and Ghil 1999; Robertson et al. 2015). Precipitation and both  
248 maximum and minimum temperature are simulated through bootstrapping from the historical  
249 record conditional on the simulated WRs. Noise is added to resampled heavy precipitation events

250 to ensure that simulated extreme events can exceed those in the observations. To capture  
251 thermodynamic mechanisms of climate change, the weather generator post-processes simulated  
252 precipitation and temperature data to reflect patterns of warming and thermodynamic scaling of  
253 precipitation rates with that warming (i.e., precipitation intensification).

254 This model was developed for 20 separate river basins across the entire state of  
255 Massachusetts (at the 8-digit Hydrologic Unit Code: Huc8 level), using gridded (~6 km) daily  
256 precipitation and maximum and minimum temperature between January 1, 1950 and December  
257 31, 2013 from the dataset developed by Livneh et al. (2015). For every HUC8 watershed, the  
258 model was used to simulate 100 ensemble members, each 64-years long (the length of the  
259 instrumental record), for temperature changes that range from 0°F to 8°F (0 °C to 4.44 °C)  
260 warming at 0.5°F (0.28°C) increments (17 warming scenarios altogether). This was the range of  
261 warming projected in the CMIP5 ensemble of future projections across the state of  
262 Massachusetts for all emission scenarios.

263 For each level of warming, extreme precipitation simulated by the model was scaled  
264 upwards using a quantile mapping approach. Specifically, the daily, non-zero precipitation  
265 distribution for each grid cell was stretched such that the 99.9<sup>th</sup> percentile was increased at the  
266 theoretical Clausius-Clapeyron (CC) scaling rate (~7% per °C warming), which is the rate at  
267 which the water holding capacity of the atmosphere increases with warming (Held and Soden  
268 2006). If all other factors controlling precipitation intensity remain unchanged, it is often  
269 assumed that extreme precipitation will scale with temperature at this same rate (Allan and  
270 Soden 2008; Allen and Ingram 2002). The reasoning is that under conditions that lead to extreme  
271 precipitation (i.e., near saturated atmospheric conditions; intense surface convergence and uplift),  
272 changes in atmospheric moisture content will translate directly to changes in precipitation

273 amount. A separate analysis of extreme precipitation scaling across the Northeast US was used to  
274 support this choice (Najibi, Mukhopadhyay, and Steinschneider 2022; Steinschneider and Najibi  
275 2022a). Mean precipitation was held at historical levels in these scenarios.

276 The climate change mechanisms that lead to hydrologic impact are categorized into  
277 thermodynamic or dynamic impacts of climate change. Thermodynamic impacts are directly  
278 related to the temperature change of the atmosphere. Thermodynamic modes include snow  
279 accumulation and melt, higher evapotranspiration, and more intense precipitation due to an  
280 increase in the moisture holding capacity of atmosphere. Dynamic atmospheric mechanisms refer  
281 to the frequency of weather regimes (i.e., shifts in atmospheric circulation) (Steinschneider and  
282 Najibi 2022), which are significantly more uncertain than thermodynamic change (Shepherd,  
283 2014; Pfahl et al., 2017). The climate scenarios included in this analysis only reflect mechanisms  
284 of thermodynamic climate change, which are direct responses of the climate to warming and are  
285 often deemed some of the most credible projections of future climate (Pfahl et al., 2017). In this  
286 study we used the SWG simulations over the Squannacook River basin as the forcing to our  
287 hydrologic model, described next. Steinschneider and Najibi (2022a) found a substantial increase  
288 in the extreme rainfall intensity in the scenarios used for this study.

289

### 290 **2.3. Stochastic Watershed Model**

291 In this work we employ a SWM to translate scenarios of climate from the SWG into  
292 streamflow simulations. SWMs use a deterministic watershed model (DWM) to simulate the  
293 hydrologic response to climate, and then re-introduce errors back into the DWM prediction to  
294 address the bias in extreme flows (Vogel 2017). In this work, we adopt the SWM developed in  
295 Shabestanipour et al. (2023), which was verified and validated for the Squannacook River basin.

296 As described above, the USGS National Hydrologic Model Precipitation Runoff Modeling  
297 System (NHM-PRMS) (Regan et al. 2019) segment for the Squannacook River was used as the  
298 core DWM.

299 To add error back to the DWM predictions, the SWM in Shabestanipour et al. (2023) fits  
300 an autoregressive (AR(3)) model to the log-ratio (denoted  $\lambda$ ) of simulated and observed  
301 streamflow from the NHM-PRMS. Simulations of new log-ratios are then generated by first  
302 bootstrapping residuals from the fitted AR model, then using those resampled residuals in the  
303 AR model to re-introduce autocorrelation, and finally using those simulated log-ratios to adjust  
304 DWM simulated flows into a stochastic trace of simulated streamflow. There is also a separate  
305 bias correction factor (BCF) applied to address biases that can arise when operating on log-  
306 transformed flows. All equations for this model can be found in *Figure 1*.

307 We note that the PRMS model and the SWM in Shabestanipour et al. (2023) were both  
308 calibrated using observed meteorological data from the Daymet dataset (Thornton et al. 2016),  
309 but the SWG produces weather traces based on the meteorological data in Livneh et al. (2015).  
310 This change in input data introduces a bias to our simulated streamflows, which we address using  
311 a quantile mapping bias correction calibrated over the historical period (see Supporting  
312 Information; Teegavarapu, Salas, and Stedinger 2019).

313 Ultimately, we force the DWM with the 17 different warming scenarios from the SWG,  
314 each containing 100 ensemble members, for a total of 1,700 separate time series of deterministic  
315 streamflow predictions. We then used the SWM to simulate 10,000 stochastic streamflow traces  
316 for each of these 1,700 realizations, producing a super ensemble of 17,000,000 streamflow  
317 traces. Here, each of the 17 warming scenarios (which capture future climate change uncertainty)

318 have 1,000,000 hydrologic simulations that capture both natural climate variability and  
319 hydrologic model uncertainty.

320

#### 321 **2.4. Risk-of-Failure Design Criterion**

322 By integrating the SWG and SWM above, we can simulate a super ensemble of  
323 streamflow traces associated with 17 separate levels of future warming. However, these traces  
324 (which are each 64 years long) reflect a different step change in temperature rather than gradual,  
325 transient scenarios of warming. Therefore, the ensemble of 1,000,000 streamflow traces  
326 associated with each level of warming can be used to calculate the stationary risk of  
327 infrastructure failure for a particular level of warming, but they cannot be directly used to  
328 calculate the risk of failure over a T-year planning horizon during which temperatures gradually  
329 warm.

330 We address this challenge by first calculating the stationary risk of failure for each  
331 warming scenario generated by the SWG-SWM ensemble, and then integrate this risk of failure  
332 over transient pathways of warming projected by GCMs. To demonstrate this approach, let A be  
333 a particular flood magnitude of concern (e.g., the flood level that would exceed the capacity of a  
334 planned infrastructure project). We then define the probability that the flood magnitude A will  
335 not be exceeded for a particular warming scenario  $W \in (0 \text{ }^\circ\text{F} (0 \text{ }^\circ\text{C}), 8 \text{ }^\circ\text{F} (4.44 \text{ }^\circ\text{C}))$  as:

$$P(A|W) = \frac{\text{Number of years in warming scenario } W \text{ that flow } A \text{ is not exceeded}}{\text{Number of all years in scenario } W} \quad (1)$$

336

337 For a planning horizon of T years, we can then calculate the risk of infrastructure failure over  
338 that horizon as follows:

339

$$Risk (A)_T = 1 - \prod_{t=1}^T P(A|W_t) \quad (2)$$

340 Here,  $Risk (A)_T$  is the risk associated with flood A over T years, and  $W_t$  is the amount of  
341 warming at year t over the planning horizon.

342 There are two considerations in the formulation above that require discussion. First, the  
343 transient warming  $W_t$  for each year  $t$  in the planning horizon needs to be specified. For  
344 illustration, we do this using a transient projection of temperature from the GFDL-ESM2G GCM  
345 forced with two separate emission scenarios (RCP 4.5 and RCP8.5) and downscaled using the  
346 Multivariate Adaptive Constructed Analogs approach (MACA; (Abatzoglou and Brown 2012)).  
347 For each RCP, we compare the historical temperatures from this model to the predicted future  
348 temperatures and set  $W_t$  to the warming level at the end of each decade out to 2100. That is,  
349 annual values of  $W_t$  increase upwards once every decade over a planning horizon of T=77 years  
350 (assuming a starting year of 2025). In this step, we used the decadal time steps in order to both  
351 decrease the noise from interannual variability and the necessary computational power.

352 Second, the probability  $P(A|W)$  is only available for the discrete levels of warming  
353 generated by the SWG (0 °F to 8 °F at 0.5 °F increments), but  $W_t$  can reflect any level of  
354 warming occurring at year  $t$  in the planning horizon. Therefore, if  $W_t$  is between one of the  
355 increments of warming produced by the SWG, the probability  $P(A|W_t)$  is estimated by linearly

356 interpolating between the probabilities  $P(A|W)$  for SWG-informed warming levels that are  
357 directly above and below  $W_t$ .

358

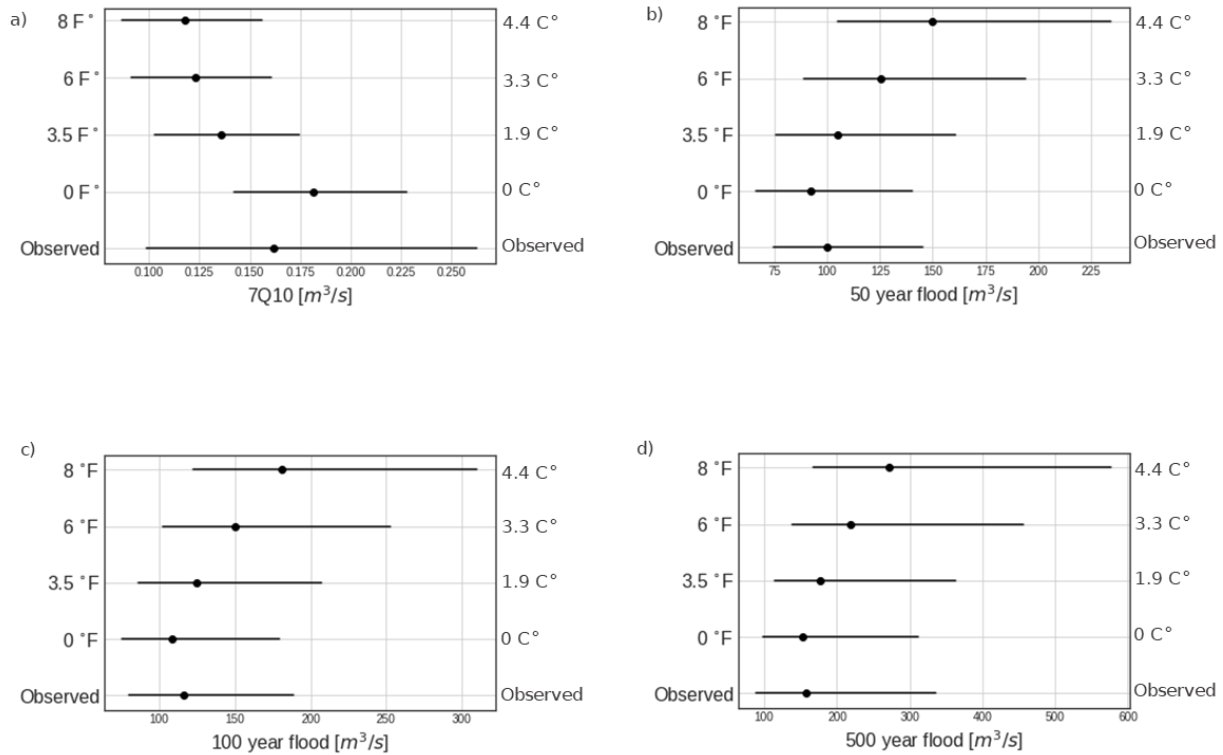
### 359 **3. Results and Discussion**

360 The integrated SWG-SWM framework described in Section 2 allows planners and  
361 engineers to track the impacts of climate change on the distribution of key design statistics for  
362 varying levels of warming or over climate change scenarios, or alternatively to evaluate the risk  
363 of a given flow being exceeded over the intended design life of a project. We address each of  
364 these two cases in turn for the Squannacook River in Sections 3.1 and 3.2 below.

#### 365 **3.1. Non-Stationary Design Events**

366 *Figure 3* compares the distribution of several common drought and flood design statistics  
367 under vary levels of warming to the observed values over the historical period (1950-2013).  
368 Observed values are derived by fitting a log-Pearson Type III distribution to the annual  
369 maximum or 7-day low flow series (Chowdhury and Stedinger 1991). For each of the flood  
370 statistics, the SWG-SWM simulations for 0 °F /°C warming closely match the observational  
371 record, producing similar median and 90% confidence intervals. This indicates that the SWG-  
372 SWM framework can replicate flood characteristics under historical conditions and suggests the  
373 model should provide reasonable projections of flood characteristics under warming conditions.  
374 The SWG-SWM framework struggles to capture the uncertainty in the estimate of the 7Q10  
375 (minimum annual 7-day average flow with 10-year recurrence interval) from the observational  
376 record, which is likely due in part to the underlying hydrologic model’s poor performance in  
377 simulating low flows in the Squannacook (Shabestanipour et al. 2023). Despite this, the SWM-

378 SWG median 7Q10 is close to the observed 7Q10 and is well within the 90% confidence interval  
 379 (see 0 °C scenario width of calculated 7Q10s in *Figure 3a*).



380  
 381 **Figure 3:** Impact of fixed warming levels on the distribution of the a) 7Q10, b) 50-year flood, c)  
 382 100-year flood, and d) 500-year flood.

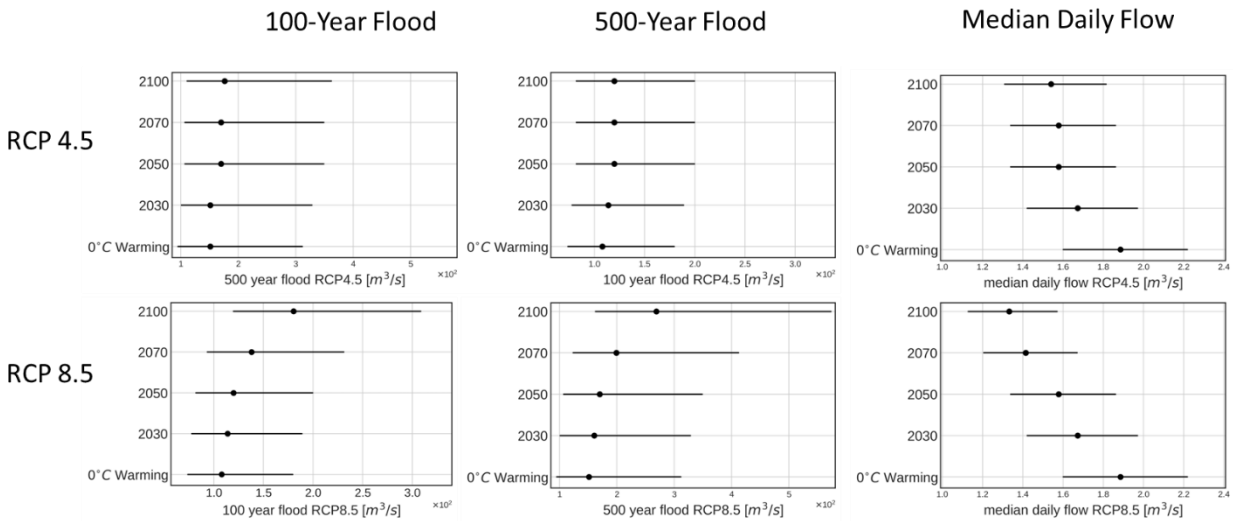
383

384 The SWG-SWM framework projects that both droughts and floods will become more  
 385 extreme as temperatures increase in the Squannacook. For example, under 4 °F (2.22 °C)  
 386 warming the SWG-SWM projects an increase in the median 100-year flood of 19% over 0 °F (0  
 387 °C) conditions, and an increase of 68% under 8 °F (4.44 °C) warming. For a fixed AEP flood, the  
 388 marginal flood magnification with respect to an increase in warming also increases, so flood  
 389 magnification is a non-linear function of warming for the Squannacook. For a fixed warming  
 390 level, the flood magnification also increases with return period. For example, under 8 °F (4.44

391 °C), the SWG-SWM projects an increase of 63%, 68%, and 78% for the 50-, 100-, and 500-year  
392 floods, respectively. There is significant uncertainty in both the observed and projected flood  
393 magnitudes, as reflected in the wide 90% confidence intervals in *Figure 3*. The projected median  
394 100- and 500-year floods are within the 90% confidence interval of the observed historical  
395 record, as estimating such extreme flood quantiles from a limited historical record includes  
396 significant uncertainty. The projected distributions of extreme floods are positively skewed, with  
397 upper tails that extend to extreme flood magnitudes, and this asymmetry grows with warming  
398 conditions.

399 While the fixed warming levels in *Figure 3* are useful to track the basin response to  
400 warming, climate change is expected to evolve through the course of the 21<sup>st</sup> century and most  
401 planning exercises use climate scenarios, such as the representative concentration pathways  
402 (RCPs) (Van Vuuren et al. 2011). Figure 4 plots the evolution of the median daily flow, the 100-  
403 year flood, and the 500-year flood for RCP4.5 and RCP8.5 by decade through 2100, by mapping  
404 the GCM-projected temperature change under each emission scenario and for each target year to  
405 a SWG-SWM warming scenario. The no-warming scenario is also shown as a baseline. The  
406 SWG-SWM framework projects a decline in the median daily flow through 2100 under both  
407 climate scenarios: a 21% decline for RCP4.5 and a 33% decline for RCP8.5. Despite this,  
408 extreme flood magnitudes are projected to increase under both RCPs. Under RCP4.5 extreme  
409 flood magnification is modest, with a median flood magnification of 15% for the 100-year flood  
410 and 17% for the 500-year flood by 2100. Even by the end of the century, under RCP4.5 the  
411 median 100- and 500-year flood magnitudes are well within the 90% confidence interval for the  
412 no-warming case, reflecting both the uncertainty in extreme flood estimation and the limited  
413 impact of modest warming on extreme flood quantiles (see also *Figure 3*). RCP8.5 sees more

414 substantial shifts in the distribution of extreme floods by 2100, with a 67% and 77% increase in  
 415 the 100- and 500-year median floods, respectively. Flood magnification quickens after 2050,  
 416 when RCP8.5 projects a more rapid rise in global warming levels. By 2100 under RCP8.5, the  
 417 SWG-SWM framework projects that the 100-year flood magnitude will exceed the estimated  
 418 500-year flood over the historical period. This behavior is due to the fact that global temperature  
 419 change of the RCP8.5 scenario starts to vary significantly from the RCP4.5 scenario after 2050  
 420 (Ansuategi et al. 2015).



421 **Figure 4:** Design floods and median daily flows by decade under RCP4.5 and RCP8.5 and under  
 422 0 °F/°C warming.  
 423

424

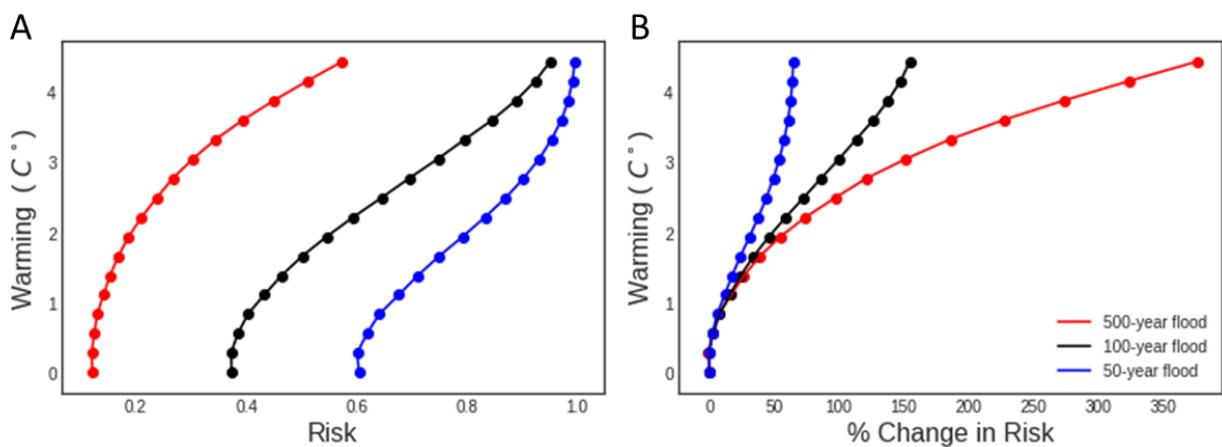
425 Previous studies in the region project approximately a 30% increase in the 100-year flood in  
 426 western and central Massachusetts under RCP8.5 (Siddique and Palmer 2021; Siddique et al.  
 427 2020), which is less extreme than our results. Both our study and previous studies suggest greater  
 428 increase around the end of the century. Our results for RCP4.5 are in general agreement with  
 429 previous work, which estimate an approximate 15% increase of the 100-year flood under this  
 430 warming trajectory (Siddique and Palmer 2021).

431

### 432 3.2. Risk of Failure

433 *Figure 4* provides a useful demonstration of shifting extremes in a non-stationary world  
434 by tracking changes in common design statistics over time for different climate scenarios. *Figure*  
435 *4* also highlights the deficiency of the “return period” or the AEP as a concept for  
436 communicating risk under non-stationarity. The median 100-year flood can be expected to  
437 change over the design life of infrastructure built today due to climate change (Milly et al. 2002).  
438 In the case of the Squannacook, the 100-year flood is expected to get larger over time. Planning  
439 for the 100-year flood today risks under-design, whereas planning for the 100-year flood at the  
440 end of the planning horizon risks over-design. Non-stationary return periods have been proposed  
441 (Olsen, Lambert, and Haines 1998; Salas and Obeysekera 2014), but their meaning can be  
442 difficult to interpret. A more natural design criteria is risk (or conversely, reliability), whose  
443 interpretation is the same under stationary or non-stationary conditions (Read and Vogel 2015).

444

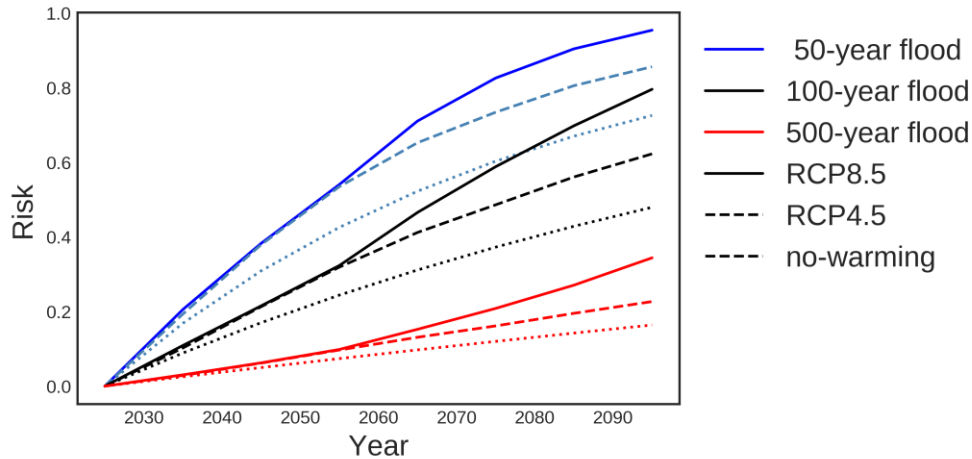


445

446 **Figure 5:** A) The impact of warming on the risk of no-warming design events over a 50-year  
447 design life. B) Percent change in risk of no-warming design events over a 50-year design life.

448

449 *Figure 5* reports the relationship between risk and various fixed return period floods  
450 under a range of warming conditions, for a 50-year design life. *Figure 5A* illustrates how the risk  
451 of the no-warming 50-year, 100-year, and 500-year floods change for the Squannacook as  
452 temperatures increase. As expected from equation 2, the risk of the no-warming 50-, 100-, and  
453 500-year events being exceeded in a 50-year design life under the no-warming case are about  
454 60%, 40%, and 10%, respectively. As temperatures warm in the Squannacook, the risk of each  
455 design event being exceeded increases substantially, with 4.5 °F of warming the risk of the no-  
456 warming 100-year event exceeding the theoretical risk of the 50-year flood in stationary  
457 conditions. The relationship between risk and warming is nonlinear and varies by return period.  
458 At low warming levels, the risk of the 50-year flood increases more rapidly with temperature in  
459 absolute terms than risk of the 500-year event. However, the opposite is true at high warming  
460 levels, with the 500-year flood's risk increasing with temperature faster than the 50-year flood.  
461 *Figure 5B* shows the percent change in risk for the three design events under varying degrees of  
462 warming. For a fixed level of warming, the relative increase in risk grows with return period. For  
463 example, under 6 °F of warming, the risk of the 50-year flood has increased 58% while the 500-  
464 year flood risk has increased 186%. As temperatures increase, the relative increase in the risk of  
465 the 500-year flood grows rapidly, while the relative increase in the risk of the 50-year event  
466 stagnates as it approaches 100% risk in absolute terms (e.g., near certainty that it will be  
467 exceeded over the 50-year design life).



468  
 469 **Figure 6:** Accumulated risk of no-warming design events over the 21<sup>st</sup> century for the RCP4.5,  
 470 RCP8.5, and no-warming scenarios.

471

472 *Figure 6* reports the accumulated risk of various design floods (computed under no  
 473 warming), being exceeded over time under three future climate scenarios: no-warming, RCP4.5,  
 474 and RCP8.5. Risk increases over time, as each year there is a chance the specified design flow  
 475 will be exceeded. The risk increases faster for less-extreme floods (e.g., 50-year flood), as each  
 476 year there is a higher probability that that flow level will be exceeded. Risk also grows more  
 477 quickly for the two warming scenarios than for the no-warming case, because the SWG-SWM  
 478 projects that increasing temperatures will increase extreme floods. The difference in risk between  
 479 RCP4.5 and the no-warming case is notable, given the SWG-SWM framework projects only  
 480 modest increases in extreme floods under RCP4.5 (see Figure 4). This highlights that even small  
 481 increases in annual flood risk compound over time to yield substantial differences in risk over a  
 482 long planning horizon. There is very little difference between RCP4.5 and RCP8.5 through 2050,  
 483 because those two climate scenarios follow similar warming trajectories until mid-century. After  
 484 2050, risk accumulates quicker for RCP8.5 than RCP4.5, as the SWM-SWG projects that floods  
 485 will become more extreme under RCP8.5 than RCP4.5. *Figure 6* suggests that the choice of

486 climate scenario (RCP4.5 vs. RCP8.5) does not meaningfully impact flood risk if the planning  
487 horizon terminates around 2050, but that after 2050 the choice of climate scenario can impact the  
488 projected flood risk.

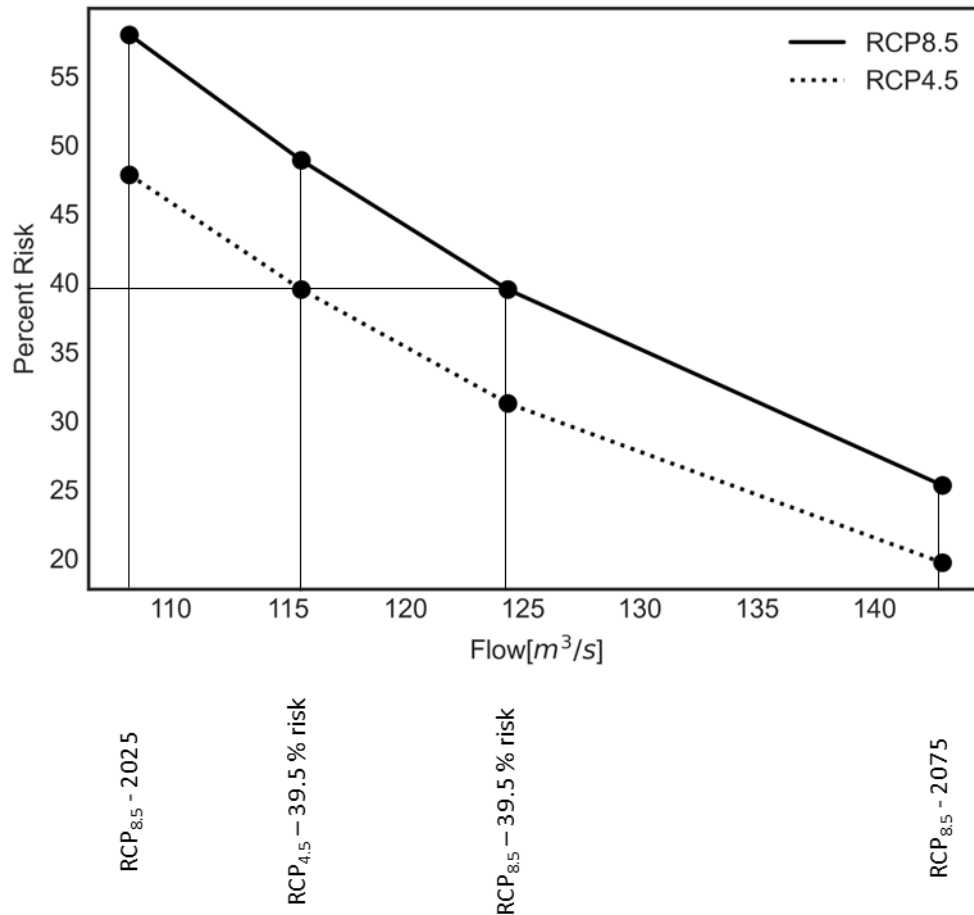
489 To further explore generalizability of this framework we implemented the SWG-SWM  
490 integration process for the Shasta River basin in California, United States. We have included the  
491 results of secondary basin's analysis in the supplementary material. Implementation of the  
492 framework on a second basin supports the applicability of this method on basins with different  
493 hydrologic characteristics.

### 494 **3.3. Risk-based Decision Making using the SWM-SWG framework**

495 To demonstrate the application of the SWG-SWM framework for risk-based decision  
496 making, we consider the design of culvert with a 50-year design life being constructed in 2025.  
497 In Massachusetts, the recommended design flow for a culvert is the 100-year flood  
498 (Massachusetts Department of Transportation 2020). Under stationary conditions, this implies a  
499 39.5% risk over the design life. When designing a culvert in non-stationary conditions, the  
500 planner has at least three choices in selecting a design flow: (1) design to the current 100-year  
501 flood (here represented by the no-warming case), (2) design to the 100-year flood at the end of  
502 the design life under a climate scenario, or (3) design to a flow that matches the desired risk  
503 implied by current design standards (i.e., 39.5%). *Figure 7* plots the design-life risk associated  
504 with each of those options for RCP4.5 and RCP8.5 versus the design flow. For choice 1 and 2  
505 the associated risk of the design flow is calculated by equation (2) and the third design flow was  
506 found by a grid search for the associated risks of flows in between the two initial flows. Here the  
507 design flow can be considered a proxy for cost, albeit an approximate and non-linear one. Each  
508 line represents an alternative climate scenario, which is uncertain and represents a design choice.  
509 An ideal solution (given a climate scenario) would be one in the lower left of *Figure 7*: a low-

510 risk solution with a small design flow and consequently a smaller cost. Unfortunately, the ideal is  
511 not possible, and a compromise must be selected.

512



513

514 **Figure 7:** Risk over a 50-year design life under RCP4.5 and RCP8.5 for alternative design flows.

515

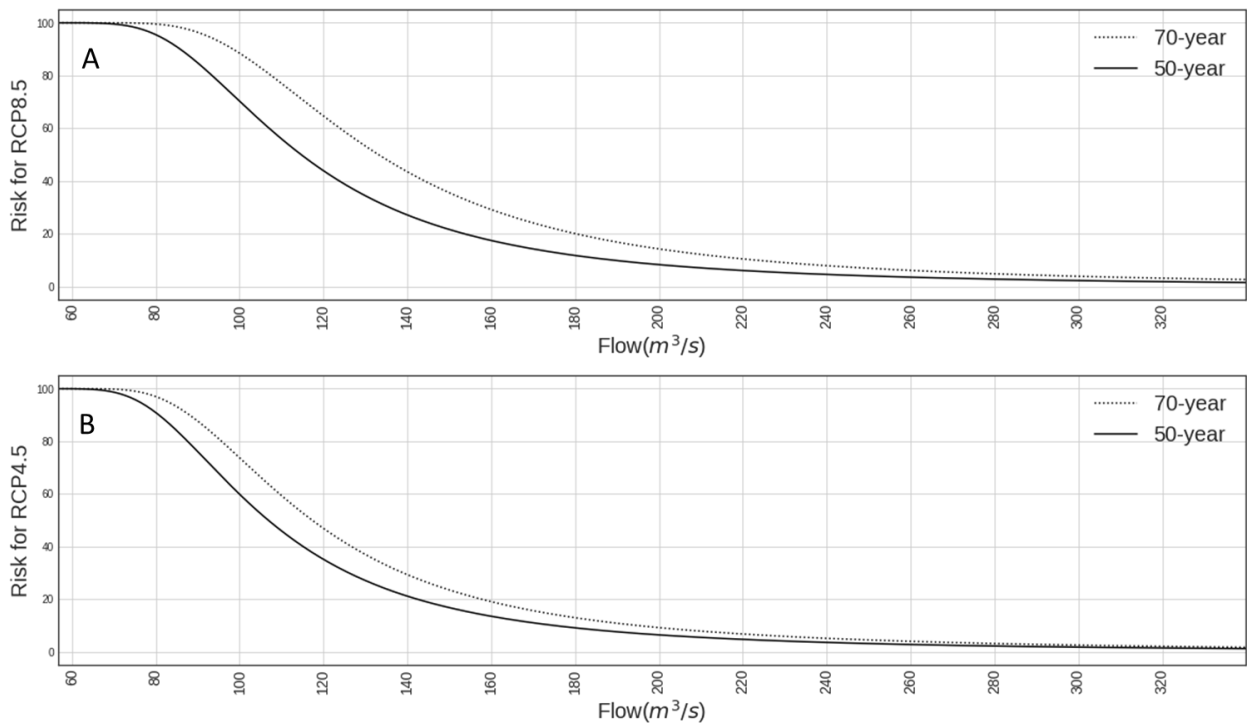
516 The current (no-warming) 100-year flood is roughly 3,800 cfs ( $107 m^3/s$ ) and  
517 corresponds to a life-time risk of about 40% under stationary conditions. However, the risk of the  
518 current design flow is substantially higher under climate scenarios: rising to 48% under RCP4.5  
519 and 58% under RCP8.5. Thus, utilizing the current 100-year flood results in under-design and  
520 unacceptable levels of risk in the Squannacook under climate change, according to design

521 standards. Instead, planners may opt to design for the 100-year flood at the end of the design life,  
522 in this case 2075. As the SWG-SWM framework projects increasing flood magnitudes through  
523 the course of the 21st century, this may be perceived as a sensible, conservative choice.  
524 However, this will result in significantly lower risk than desired in the design codes. Under  
525 RCP8.5, the SWG-SWM projects the 2075 100-year flood to be about 5,000 cfs ( $141.5 \text{ m}^3/\text{s}$ ),  
526 corresponding to a risk of 25.3%. On its face, a lower risk seems desirable, but it also represents  
527 a significant over design: a flow of about 4,400 cfs ( $124.6 \text{ m}^3/\text{s}$ ) achieves the desired 39.5% risk  
528 under RCP8.5. If the actual warming is less extreme than RCP8.5, which is likely (Hausfather et  
529 al. 2022; Voosen 2022; Hausfather and Peters 2020), then the overdesign and consequently the  
530 regret will be even more extreme. A thorough economic analysis of the costs of over- vs. under-  
531 design is beyond the scope of this simple example, but if the design standards reflect societal  
532 risk-tolerance, then selecting the 100-year flood at the end of the design life reflects over design,  
533 and a potential inefficient use of resources that might be spent elsewhere in support of other  
534 societal objectives.

535 As shown in *Figure 4*, RCP4.5 projects more moderate changes to extreme floods over  
536 the 21<sup>st</sup> century than RCP8.5. The SWG-SWM projects the 100-year flood to be about 4,200 cfs  
537 ( $118.9 \text{ m}^3/\text{s}$ ) in 2075 under RCP4.5, while the flow required to achieve the desired 39.5% is  
538 about 4,100 cfs ( $116 \text{ m}^3/\text{s}$ ). Thus, designing for the 100-year flood in 2075 under RCP4.5  
539 represents only a slight overdesign, with an actual risk of 35.7%. Of course, the future will not  
540 follow exactly the scenario selected for planning, so it is instructive to consider the loss or gain  
541 of risk if an alternative climate scenario occurs than the one planned for. For example, if the  
542 2075 100-year flood from RCP8.5 is used for planning, but RCP4.5 actually occurs, the associate  
543 risk is 19.7% compared to the desired 39.5% and the infrastructure would be designed for a flow

544 that is nearly 1,000 cfs ( $28.3 \text{ m}^3/\text{s}$ ) larger than required to achieve the desired risk. The regret of  
545 overdesign could be quantified monetarily in a more applied problem. In contrast, if the design  
546 flow is selected to achieve 39.5% risk under RCP8.5, and RCP4.5 actually occurs, the associated  
547 risk would be 31.3% rather than the desired 39.5% and the infrastructure would be designed to a  
548 flow only about 300 cfs ( $8.5 \text{ m}^3/\text{s}$ ) larger than required. Thus, if planning for RCP8.5, adopting  
549 a risk framing rather than the end-of-horizon 100-year flood reduces the regret of overdesign  
550 substantially. This result arises in part because RCP4.5 and RCP8.5 follow similar trajectories  
551 through 2050, so the flow associated with a life-time risk of 39.5% is quite similar, even if their  
552 2075 100-year floods are quite different.

553



554

555 **Figure 8:** Risk versus flood magnitude for infrastructure built in 2025 with either a 50-year or  
556 70-year design life, under a) RCP8.5 and b) RCP4.5.

557

558 Figure 8 plots risk vs. flow for two planning horizons (50 and 70 years starting in 2025)  
559 and two climate scenarios (RCP4.5 and RCP8.5). This diagram can be used by practitioners to  
560 identify a design flow associated with a desired risk, planning horizon, and climate scenario, or  
561 alternatively a practitioner could identify the risk associated with a given flow, planning horizon,  
562 and climate scenario. The 50-year planning horizon risk profiles are similar between RCP4.5 and  
563 RCP8.5, largely because their warming trajectories are quite close into the middle of the 21<sup>st</sup>  
564 century. Because both RCP4.5 and RCP8.5 project rising temperatures through the end of the  
565 21<sup>st</sup> century, the SWM-SWM projects increasing flood magnitudes through 2100 (see Figure 4).  
566 Thus, the longer the planning horizon stretches into the future, the more the risk-profile shifts to  
567 the right (greater flows associated with a fixed risk). The relative shift in the risk profile between  
568 the 50- and 70-year planning horizon is greater for RCP8.5 than RCP4.5, reflecting the greater  
569 projected late-century warming under RCP8.5. Using the simulation ensemble from the SWG-  
570 SWM framework, Figure 8 can be expanded to include alternative planning horizons or new  
571 climate scenarios.

572  
573 **4. Conclusions**

574 Climate change is expected to alter the distribution and arrival of hydrologic extremes,  
575 and this presents a significant challenge to long-term water resources planning and management.  
576 Mapping the hydrologic response to changing climate drivers is challenging, in part because of a  
577 mismatch in the scale and focus of common climate and hydrologic models with the needs of  
578 local planners. More fundamentally, non-stationarity renders the interpretation of common  
579 design statistics, like the 100-year flood, technically ambiguous and of dubious practical value.  
580 To address both issues, this work presents a computational framework for risk-based decision

581 making at the basin-scale, composed of a Stochastic Weather Generator (SWG) and a Stochastic  
582 Watershed Model (SWM). The SWG is used to produce many synthetic weather sequences  
583 reflecting different levels of warming and associated intensification of extreme precipitation,  
584 while using abstractions of dynamic atmospheric mechanisms to capture key signals of natural  
585 climate variability. The SWM captures the hydrologic response to changing climate forcing,  
586 correcting bias in the deterministic hydrologic models' representation of extreme flows by  
587 properly capturing the variance of daily streamflow. The integrated SWG-SWM framework is  
588 applied to the Squannacook River basin in Massachusetts to illustrate the impact of climate  
589 change on the distribution of hydrologic extremes and use of risk in hydrologic design.

590 For the Squannacook, the SWG-SWM framework projects that warming temperatures  
591 will produce more extreme floods and low flow events. The increase in flood magnitude is non-  
592 linear with respect to warming: the marginal increase in flood magnitude with respect to an  
593 increase in temperature increases with the warming level. The increase in flood magnitude with  
594 warming is also greater for more extreme floods: the relative increase of the 500-year flood is  
595 greater than the relative increase of the 100-year flood for a fixed warming level. Still, the  
596 uncertainty in extreme floods under no warming is sufficiently large to encompass median  
597 estimates of extreme flooding under a high degree of warming.

598 A similar non-linear pattern is seen for the risk of failure of a specified flood magnitude  
599 over a given planning horizon. For smaller flood magnitudes, the risk saturates towards unity for  
600 moderate horizons (e.g.,  $T=50$  years) as it becomes near certain that those events will be  
601 exceeded, while for larger floods the risk grows exponentially (on a percentage basis).  
602 Importantly, the accumulated risk associated with flooding is similar between moderate and high  
603 emission scenarios during the first half of the 21<sup>st</sup> century because the two scenarios follow

604 similar warming trajectories until around 2050. This result has large implications for reducing  
605 regret in hydrologic design. Our results show that basing hydrologic designs on return period  
606 estimates at either the beginning or the end of a planning horizon can lead to large regret (under-  
607 or over-design), especially if a different climate future occurs than the one used to guide design.  
608 This regret can be reduced if design is based on a risk framing, largely because different  
609 emission scenarios (RCP4.5 and RCP8.5) follow similar warming trajectories through mid-  
610 century, so the flow associated with a given life-time risk of failure is more similar than the end-  
611 of-horizon return period events.

612 While the SWG-SWM framework to support risk-based hydrologic design proposed in this  
613 work shows promise, several limitations of the method require discussion. First, the SWG is  
614 designed to propagate key signals of climate change into large ensembles of future weather for  
615 risk analysis, but the model is not governed by the physical laws of the climate system and  
616 therefore may produce weather ensembles that are not physically plausible, especially for  
617 extreme climate change scenarios. In addition, the SWG was only used in this study to create  
618 scenarios of warming and extreme precipitation intensification, without consideration of other  
619 signals of potential climate change (e.g., shifts in seasonality, changes in mean precipitation,  
620 etc.). A more in-depth analysis could use the SWG to expand the set of scenarios tested, or  
621 alternatively, multiple single model initial condition large ensembles (SMILES, Lehner et al.  
622 2020) could be used as the basis for the weather ensembles in our risk-based framework. In  
623 either case, multiple signals of future climate change beyond just warming could interact to  
624 influence hydrologic risk-of-failure, and these effects should be disentangled (e.g., using  
625 variance decomposition; (Steinschneider et al. 2023) to understand the relative importance of  
626 different climate change signals on risk. This effort will be the focus of future work.

627 A second important limitation of this work is the assumption in the SWM that the error  
628 structure observed historically can be used to propagate hydrologic model uncertainty under new  
629 climate conditions. Climate change will alter the frequency, timing, and intensity of hydrologic  
630 model states, activate model components in configurations not seen in the historical record, and  
631 change the way meteorological forcing is converted to streamflow. These changes could alter the  
632 structure and distribution of hydrologic model errors, although it is difficult to anticipate these  
633 changes because no future observations are available against which to estimate shifts in the error  
634 distribution. One promising approach to address this challenge is to link the error distribution in  
635 SWMs to hydrologic model state variables, so that changes in the frequency of different states  
636 under climate change trigger an associate shift in the error distribution. This is an active topic of  
637 ongoing research. Another limitation of this work is we do not consider any land-use change for  
638 future scenarios. Future work for long-term decision making should consider various  
639 combinations of land-use change scenarios and warming scenarios.

640 More broadly, we argue that there is a need for practitioners in hydrologic engineering to  
641 move away from conventional approaches to design such as return period-based design event  
642 estimation. These techniques, while suitable in the past, are no longer justified given the  
643 accelerating rate at which the risk of extreme events is changing, and the propensity of these  
644 methods to lead to the future under- or over-design of infrastructure. Instead, we argue that risk-  
645 based approaches like the one forwarded in this work and advocated elsewhere (Read and Vogel  
646 2015) provides an intuitive approach that is well-suited for a future in which risk is highly  
647 uncertain and dynamic. We recognize that the legacy of return period event-based design is  
648 entrenched in the current state of practice for hydrologic engineering. Therefore, as new  
649 methodologies emerge to support risk-based approaches, we argue that equal or more effort is

650 needed to advocate for their use in practice, including the introduction of such alternative  
651 approaches in undergraduate and graduate school curricula.

652

653 **Data Availability Statement**

654 The data and code for the analysis in this study is available at:

655 <https://doi.org/10.5281/zenodo.8393390>

656

657

658 **References**

659

- 660 Abatzoglou, John T., and Timothy J. Brown. 2012. "A Comparison of Statistical Downscaling  
661 Methods Suited for Wildfire Applications: STATISTICAL DOWNSCALING FOR  
662 WILDFIRE APPLICATIONS." *International Journal of Climatology* 32 (5): 772–80.  
663 <https://doi.org/10.1002/joc.2312>.
- 664 Allan, Richard P., and Brian J. Soden. 2008. "Atmospheric Warming and the Amplification of  
665 Precipitation Extremes." *Science* 321 (5895): 1481–84.  
666 <https://doi.org/10.1126/science.1160787>.
- 667 Allen, Myles R., and William J. Ingram. 2002. "Constraints on Future Changes in Climate and  
668 the Hydrologic Cycle." *Nature* 419 (6903): 224–32. <https://doi.org/10.1038/nature01092>.
- 669 Balting, Daniel F., Amir AghaKouchak, Gerrit Lohmann, and Monica Ionita. 2021. "Northern  
670 Hemisphere Drought Risk in a Warming Climate." *Npj Climate and Atmospheric Science*  
671 4 (1): 61. <https://doi.org/10.1038/s41612-021-00218-2>.
- 672 Chowdhury, Jahir Uddin, and Jery R. Stedinger. 1991. "Confidence Interval for Design Floods  
673 with Estimated Skew Coefficient." *Journal of Hydraulic Engineering* 117 (7): 811–31.  
674 [https://doi.org/10.1061/\(ASCE\)0733-9429\(1991\)117:7\(811\)](https://doi.org/10.1061/(ASCE)0733-9429(1991)117:7(811)).
- 675 Cooley, Daniel. 2012. "Return Periods and Return Levels under Climate Change." In *Extremes  
676 in a Changing Climate: Detection, Analysis and Uncertainty*, 97–114. Springer.
- 677 Douglas, Ellen M, Richard M Vogel, and Charles N Kroll. 2002. "Impact of Streamflow  
678 Persistence on Hydrologic Design." *Journal of Hydrologic Engineering* 7 (3): 220–27.
- 679 Farmer, William H, and Richard M Vogel. 2016. "On the Deterministic and Stochastic Use of  
680 Hydrologic Models." *Water Resources Research* 52 (7): 5619–33.
- 681 Fernández, Bonifacio, and José D Salas. 1999. "Return Period and Risk of Hydrologic Events. I:  
682 Mathematical Formulation." *Journal of Hydrologic Engineering* 4 (4): 297–307.
- 683 Fowler, Hayley J, Stephen Blenkinsop, and Claudia Tebaldi. 2007. "Linking Climate Change  
684 Modelling to Impacts Studies: Recent Advances in Downscaling Techniques for  
685 Hydrological Modelling." *International Journal of Climatology: A Journal of the Royal  
686 Meteorological Society* 27 (12): 1547–78.
- 687 Gumbel, Emil Julius. 1941. "The Return Period of Flood Flows." *The Annals of Mathematical  
688 Statistics* 12 (2): 163–90.
- 689 Haghhighatafshar, Salar, Per Becker, Steve Moddemeyer, Andreas Persson, Johanna Sörensen,  
690 Henrik Aspegren, and Karin Jönsson. 2020. "Paradigm Shift in Engineering of Pluvial  
691 Floods: From Historical Recurrence Intervals to Risk-Based Design for an Uncertain  
692 Future." *Sustainable Cities and Society* 61: 102317.
- 693 Hausfather, Zeke, Kate Marvel, Gavin A. Schmidt, John W. Nielsen-Gammon, and Mark  
694 Zelinka. 2022. "Climate Simulations: Recognize the 'Hot Model' Problem." *Nature* 605  
695 (7908): 26–29. <https://doi.org/10.1038/d41586-022-01192-2>.
- 696 Hausfather, Zeke, and Glen P. Peters. 2020. "RCP8.5 Is a Problematic Scenario for near-Term  
697 Emissions." *Proceedings of the National Academy of Sciences* 117 (45): 27791–92.  
698 <https://doi.org/10.1073/pnas.2017124117>.
- 699 Hawcroft, Matt, Ella Walsh, Kevin Hodges, and Giuseppe Zappa. 2018. "Significantly Increased  
700 Extreme Precipitation Expected in Europe and North America from Extratropical  
701 Cyclones." *Environmental Research Letters* 13 (12): 124006.  
702 <https://doi.org/10.1088/1748-9326/aaed59>.
- 703 Hayhoe, Katharine, Donald J. Wuebbles, David R. Easterling, David W. Fahey, Sarah Doherty,  
704 James P. Kossin, William V. Sweet, Russell S. Vose, and Michael F. Wehner. 2018.  
705 "Chapter 2 : Our Changing Climate. Impacts, Risks, and Adaptation in the United States:  
706 The Fourth National Climate Assessment, Volume II." U.S. Global Change Research  
707 Program. <https://doi.org/10.7930/NCA4.2018.CH2>.

708 Held, Isaac M., and Brian J. Soden. 2006. "Robust Responses of the Hydrological Cycle to  
709 Global Warming." *Journal of Climate* 19 (21): 5686–99.  
710 <https://doi.org/10.1175/JCLI3990.1>.

711 Intergovernmental Panel On Climate Change (Ippcc). 2023. *Climate Change 2022 – Impacts,  
712 Adaptation and Vulnerability: Working Group II Contribution to the Sixth Assessment  
713 Report of the Intergovernmental Panel on Climate Change*. 1st ed. Cambridge University  
714 Press. <https://doi.org/10.1017/9781009325844>.

715 Kendon, Elizabeth J., Nikolina Ban, Nigel M. Roberts, Hayley J. Fowler, Malcolm J. Roberts,  
716 Steven C. Chan, Jason P. Evans, Giorgia Fosser, and Jonathan M. Wilkinson. 2017. "Do  
717 Convection-Permitting Regional Climate Models Improve Projections of Future  
718 Precipitation Change?" *Bulletin of the American Meteorological Society* 98 (1): 79–93.  
719 <https://doi.org/10.1175/BAMS-D-15-0004.1>.

720 Koutsoyiannis, D., and A. Montanari. 2022. "Bluecat: A Local Uncertainty Estimator for  
721 Deterministic Simulations and Predictions." *Water Resources Research* 58 (1).  
722 <https://doi.org/10.1029/2021WR031215>.

723 Kyselý, Jan, Zuzana Rulfová, Aleš Farda, and Martin Hanel. 2016. "Convective and Stratiform  
724 Precipitation Characteristics in an Ensemble of Regional Climate Model Simulations."  
725 *Climate Dynamics* 46 (1–2): 227–43. <https://doi.org/10.1007/s00382-015-2580-7>.

726 Lehner, Flavio, Clara Deser, Nicola Maher, Jochem Marotzke, Erich M. Fischer, Lukas Brunner,  
727 Reto Knutti, and Ed Hawkins. 2020. "Partitioning Climate Projection Uncertainty with  
728 Multiple Large Ensembles and CMIP5/6." *Earth System Dynamics* 11 (2): 491–508.  
729 <https://doi.org/10.5194/esd-11-491-2020>.

730 Livneh, Ben, Theodore J Bohn, David W Pierce, Francisco Munoz-Arriola, Bart Nijssen, Russell  
731 Vose, Daniel R Cayan, and Levi Brekke. 2015. "A Spatially Comprehensive,  
732 Hydrometeorological Data Set for Mexico, the US, and Southern Canada 1950–2013."  
733 *Scientific Data* 2 (1): 1–12.

734 Lu, Jian, L. Ruby Leung, Qing Yang, Gang Chen, William D. Collins, Fuyu Li, Z. Jason Hou, and  
735 Xuelei Feng. 2014. "The Robust Dynamical Contribution to Precipitation Extremes in  
736 Idealized Warming Simulations across Model Resolutions: Lu et al.: Dynamic Effect on  
737 Precipitation Extreme." *Geophysical Research Letters* 41 (8): 2971–78.  
738 <https://doi.org/10.1002/2014GL059532>.

739 Maher, Nicola, Sebastian Milinski, Laura Suarez-Gutierrez, Michael Botzet, Mikhail Dobrynin,  
740 Luis Kornblueh, Jürgen Kröger, et al. 2019. "The Max Planck Institute Grand Ensemble:  
741 Enabling the Exploration of Climate System Variability." *Journal of Advances in Modeling  
742 Earth Systems* 11 (7): 2050–69. <https://doi.org/10.1029/2019MS001639>.

743 Markstrom, S.L., R.S. Regan, L.E. Hay, R.J. Viger, Richard M.T webb, Robert A. payn, and J.H.  
744 LaFontaine. 2015. "Techniques and Methods." *Techniques and Methods. Techniques  
745 and Methods*.

746 Massachusetts Department of Transportation. 2020. "LRF Bridge Manual -Bridge Site  
747 Exploration." Massachusetts Department of Transportation. [https://www.mass.gov/info-  
748 details/part-i-design-guidelines](https://www.mass.gov/info-details/part-i-design-guidelines).

749 Milly, P. C. D., R. T. Wetherald, K. A. Dunne, and T. L. Delworth. 2002. "Increasing Risk of  
750 Great Floods in a Changing Climate." *Nature* 415 (6871): 514–17.  
751 <https://doi.org/10.1038/415514a>.

752 Muñoz, Ángel G., Xiaosong Yang, Gabriel A. Vecchi, Andrew W. Robertson, and William F.  
753 Cooke. 2017. "A Weather-Type-Based Cross-Time-Scale Diagnostic Framework for  
754 Coupled Circulation Models." *Journal of Climate* 30 (22): 8951–72.  
755 <https://doi.org/10.1175/JCLI-D-17-0115.1>.

756 Najibi, Nasser, Sudarshana Mukhopadhyay, and Scott Steinschneider. 2021. "Identifying  
757 Weather Regimes for Regional-scale Stochastic Weather Generators." *International  
758 Journal of Climatology* 41 (4): 2456–79. <https://doi.org/10.1002/joc.6969>.

- 759 ———. 2022. "Precipitation Scaling With Temperature in the Northeast US: Variations by  
760 Weather Regime, Season, and Precipitation Intensity." *Geophysical Research Letters* 49  
761 (8): e2021GL097100. <https://doi.org/10.1029/2021GL097100>.
- 762 Najibi, Nasser, and Scott Steinschneider. 2023. "A Process-Based Approach to Bottom-Up  
763 Climate Risk Assessments: Developing a Statewide, Weather-Regime Based Stochastic  
764 Weather Generator for California Final Report."
- 765 NOAA National Centers for Environmental Information. 2022. "ETOPO 2022 15 Arc-Second  
766 Global Relief Model." NOAA National Centers for Environmental Information.  
767 <https://doi.org/10.25921/FD45-GT74>.
- 768 O’Gorman, Paul A. 2015. "Precipitation Extremes under Climate Change." *Current Climate  
769 Change Reports* 1: 49–59.
- 770 Oki, Taikan, and Shinjiro Kanae. 2006. "Global Hydrological Cycles and World Water  
771 Resources." *Science* 313 (5790): 1068–72. <https://doi.org/10.1126/science.1128845>.
- 772 Olsen, J. Rolf, James H. Lambert, and Yacov Y. Haimes. 1998. "Risk of Extreme Events Under  
773 Nonstationary Conditions." *Risk Analysis* 18 (4): 497–510. <https://doi.org/10.1111/j.1539-6924.1998.tb00364.x>.
- 774
- 775 Pfahl, Stephan, Paul A O’Gorman, and Erich M Fischer. 2017. "Understanding the Regional  
776 Pattern of Projected Future Changes in Extreme Precipitation." *Nature Climate Change*  
777 7 (6): 423–27.
- 778 Pielke, Roger A. 1999. "Nine Fallacies of Floods." *Climatic Change* 42: 413–38.
- 779 Pörtner, Hans-Otto, Debra Cynthia Roberts, Helen Adams, Ibidun Adelekan, Carolina Adler,  
780 Rita Adrian, Paulina Aldunce, et al. 2022. "Technical Summary." *Climate Change*, 37–  
781 118.
- 782 Rahat, Saiful Haque, Scott Steinschneider, John Kucharski, Wyatt Arnold, Jennifer Olzewski,  
783 Wesley Walker, Romain Maendly, Asphota Wasti, and Patrick Ray. 2022.  
784 "Characterizing Hydrologic Vulnerability under Nonstationary Climate and Antecedent  
785 Conditions Using a Process-Informed Stochastic Weather Generator." *Journal of Water  
786 Resources Planning and Management* 148 (6): 04022028.  
787 [https://doi.org/10.1061/\(ASCE\)WR.1943-5452.0001557](https://doi.org/10.1061/(ASCE)WR.1943-5452.0001557).
- 788 Read, Laura K, and Richard M Vogel. 2015. "Reliability, Return Periods, and Risk under  
789 Nonstationarity." *Water Resources Research* 51 (8): 6381–98.
- 790 Regan, R.S., K.E. Juracek, L.E. Hay, S.L. Markstrom, R.J. Viger, J.M. Driscoll, J.H. LaFontaine,  
791 and P.A. Norton. 2019. "The U. S. Geological Survey National Hydrologic Model  
792 Infrastructure: Rationale, Description, and Application of a Watershed-Scale Model for  
793 the Conterminous United States." *Environmental Modelling & Software* 111 (January):  
794 192–203. <https://doi.org/10.1016/j.envsoft.2018.09.023>.
- 795 Richardson, Clarence W. 1981. "Stochastic Simulation of Daily Precipitation, Temperature, and  
796 Solar Radiation." *Water Resources Research* 17 (1): 182–90.
- 797 Robertson, Andrew W., and Michael Ghil. 1999. "Large-Scale Weather Regimes and Local  
798 Climate over the Western United States." *Journal of Climate* 12 (6): 1796–1813.  
799 [https://doi.org/10.1175/1520-0442\(1999\)012<1796:LSWRAL>2.0.CO;2](https://doi.org/10.1175/1520-0442(1999)012<1796:LSWRAL>2.0.CO;2).
- 800 Robertson, Andrew W., Arun Kumar, Malaquias Peña, and Frederic Vitart. 2015. "Improving and  
801 Promoting Subseasonal to Seasonal Prediction." *Bulletin of the American Meteorological  
802 Society* 96 (3): ES49–53. <https://doi.org/10.1175/BAMS-D-14-00139.1>.
- 803 Salas, Jose D, and Jayantha Obeysekera. 2014. "Revisiting the Concepts of Return Period and  
804 Risk for Nonstationary Hydrologic Extreme Events." *Journal of Hydrologic Engineering*  
805 19 (3): 554–68.
- 806 Serinaldi, Francesco. 2015. "Dismissing Return Periods!" *Stochastic Environmental Research  
807 and Risk Assessment* 29: 1179–89.
- 808 Serinaldi, Francesco, and Chris G Kilsby. 2015. "Stationarity Is Undead: Uncertainty Dominates  
809 the Distribution of Extremes." *Advances in Water Resources* 77: 17–36.

810 Shabestanipour, Ghazal, Zachary Brodeur, William H. Farmer, Scott Steinschneider, Richard M.  
811 Vogel, and Jonathan R. Lamontagne. 2023. "Stochastic Watershed Model Ensembles  
812 for Long-Range Planning: Verification and Validation." *Water Resources Research* 59  
813 (2). <https://doi.org/10.1029/2022WR032201>.

814 Sharma, Ashish, Conrad Wasko, and Dennis P. Lettenmaier. 2018. "If Precipitation Extremes  
815 Are Increasing, Why Aren't Floods?" *Water Resources Research* 54 (11): 8545–51.  
816 <https://doi.org/10.1029/2018WR023749>.

817 Siddique, Ridwan, Ambarish Karmalkar, Fengyun Sun, and Richard Palmer. 2020. "Hydrological  
818 Extremes across the Commonwealth of Massachusetts in a Changing Climate." *Journal  
819 of Hydrology: Regional Studies* 32: 100733.

820 Siddique, Ridwan, and Richard Palmer. 2021. "Climate Change Impacts on Local Flood Risks in  
821 the US Northeast: A Case Study on the Connecticut and Merrimack River Basins."  
822 *JAWRA Journal of the American Water Resources Association* 57 (1): 75–95.

823 Stainforth, David A, Thomas E Downing, Richard Washington, Ana Lopez, and Mark New.  
824 2007. "Issues in the Interpretation of Climate Model Ensembles to Inform Decisions."  
825 *Philosophical Transactions of the Royal Society A: Mathematical, Physical and  
826 Engineering Sciences* 365 (1857): 2163–77. <https://doi.org/10.1098/rsta.2007.2073>.

827 Stedinger, Jery R. 1993. "Frequency Analysis of Extreme Events." *Handbook of Hydrology*.

828 Steinschneider, Scott, Jonathan D. Herman, John Kucharski, Marriah Abellera, and Peter  
829 Ruggiero. 2023. "Uncertainty Decomposition to Understand the Influence of Water  
830 Systems Model Error in Climate Vulnerability Assessments." *Water Resources Research*  
831 59 (1): e2022WR032349. <https://doi.org/10.1029/2022WR032349>.

832 Steinschneider, Scott, and Nasser Najibi. 2022a. "Observed and Projected Scaling of Daily  
833 Extreme Precipitation with Dew Point Temperature at Annual and Seasonal Scales  
834 across the Northeast United States." *Journal of Hydrometeorology*, January.  
835 <https://doi.org/10.1175/JHM-D-21-0183.1>.

836 ———. 2022b. "A Weather-Regime Based Stochastic Weather Generator for Climate Scenario  
837 Development across Massachusetts, Technical Documentation." Biological and  
838 Environmental Engineering, Cornell University. [https://eea-nescaum-dataservices-  
839 assets-  
840 prd.s3.amazonaws.com/cms/GUIDELINES/FinalTechnicalDocumentation\\_WGEN\\_2022  
841 0405.pdf](https://eea-nescaum-dataservices-assets-prd.s3.amazonaws.com/cms/GUIDELINES/FinalTechnicalDocumentation_WGEN_20220405.pdf).

842 Steinschneider, Scott, Patrick Ray, Saiful Haque Rahat, and John Kucharski. 2019. "A Weather-  
843 Regime-Based Stochastic Weather Generator for Climate Vulnerability Assessments of  
844 Water Systems in the Western United States." *Water Resources Research* 55 (8): 6923–  
845 45.

846 Stephenson, David B, Matthew Collins, Jonathan C Rougier, and Richard E Chandler. 2012.  
847 "Statistical Problems in the Probabilistic Prediction of Climate Change." *Environmetrics*  
848 23 (5): 364–72.

849 Tan, Jackson, Lazaros Oreopoulos, Christian Jakob, and Daeho Jin. 2018. "Evaluating Rainfall  
850 Errors in Global Climate Models through Cloud Regimes." *Climate Dynamics* 50: 3301–  
851 14.

852 Tebaldi, Claudia, Abigail Snyder, and Kalyn Dorheim. 2022. "STITCHES: Creating New  
853 Scenarios of Climate Model Output by Stitching Together Pieces of Existing  
854 Simulations." *Earth System Dynamics* 13 (4): 1557–1609. [https://doi.org/10.5194/esd-  
855 13-1557-2022](https://doi.org/10.5194/esd-13-1557-2022).

856 Teegavarapu, Ramesh S. V., Jose D. Salas, and Jery R. Stedinger, eds. 2019. *Statistical  
857 Analysis of Hydrologic Variables: Methods and Applications*. Reston, VA: American  
858 Society of Civil Engineers. <https://doi.org/10.1061/9780784415177>.

859 Thornton, P.E., M.M. Thornton, B.W. Mayer, Y. Wei, R. Devarakonda, R.S. Vose, and R.B.  
860 Cook. 2016. "DaymetDaymet: Daily Surface Weather Data on a 1-Km Grid for North  
861 America, Version 3." NetCDF, July, 0 MB. <https://doi.org/10.3334/ORNLDAAC/1328>.  
862 Van Vuuren, Detlef P., Jae Edmonds, Mikiko Kainuma, Keywan Riahi, Allison Thomson, Kathy  
863 Hibbard, George C. Hurtt, et al. 2011. "The Representative Concentration Pathways: An  
864 Overview." *Climatic Change* 109 (1–2): 5–31. <https://doi.org/10.1007/s10584-011-0148->  
865 z.  
866 Vogel, Richard M. 2017. "Stochastic Watershed Models for Hydrologic Risk Management."  
867 *Water Security* 1: 28–35.  
868 Voosen, Paul. 2022. "'Hot' Climate Models Exaggerate Earth Impacts." *Science* 376 (6594):  
869 685–685. <https://doi.org/10.1126/science.adc9453>.  
870 Wilks, D. S. 2002. "Realizations of Daily Weather in Forecast Seasonal Climate." *Journal of*  
871 *Hydrometeorology* 3 (2): 195–207. <https://doi.org/10.1175/1525->  
872 7541(2002)003<0195:RODWIF>2.0.CO;2.  
873 Wilks, Daniel S. 2010. "Use of Stochastic Weathergenerators for Precipitation Downscaling."  
874 *WIREs Climate Change* 1 (6): 898–907. <https://doi.org/10.1002/wcc.85>.  
875 ———. 2012. "Stochastic Weather Generators for Climate-change Downscaling, Part II:  
876 Multivariable and Spatially Coherent Multisite Downscaling." *WIREs Climate Change* 3  
877 (3): 267–78. <https://doi.org/10.1002/wcc.167>.  
878 Wilks, Daniel S, and Robert L Wilby. 1999. "The Weather Generation Game: A Review of  
879 Stochastic Weather Models." *Progress in Physical Geography* 23 (3): 329–57.  
880 Woollings, Tim. 2010. "Dynamical Influences on European Climate: An Uncertain Future."  
881 *Philosophical Transactions of the Royal Society A: Mathematical, Physical and*  
882 *Engineering Sciences* 368 (1924): 3733–56.  
883 Zappa, Giuseppe, Len C. Shaffrey, and Kevin I. Hodges. 2013. "The Ability of CMIP5 Models to  
884 Simulate North Atlantic Extratropical Cyclones\*." *Journal of Climate* 26 (15): 5379–96.  
885 <https://doi.org/10.1175/JCLI-D-12-00501.1>.  
886

887

